EPA Public Access
Author manuscript

Environ Sci Nano. Author manuscript; available in PMC 2020 July 23.

About author manuscripts | Submit a manuscript

Polypropylene-MWCNT composite degradation, release, detection, and toxicity of MWCNT during accelerated aging

Changseok Han[1,2], **E. Sahle-Demessie**[2,*], **Eunice Varughese**[2], **Honglan Shi**[3]

[1]Department of Environmental Engineering, INHA University, Incheon 22212, Korea

[2]Oak Ridge Institute for Science and Education, Oak Ridge TN, 37831, USA

[3]U.S. Environmental Protection Agency, Office of Research and Development, National Risk Management Laboratory, Cincinnati, OH 45268, USA; Missouri University of Science and Technology, Department of Chemistry, Rolla, MO 65409, USA

Abstract

Nanomaterials (NM) are incorporated into polymers to enhance their properties. However, there are a limited number of studies on the aging of these nanocomposites and the resulting potential release of NM. To characterize NM at critical points in their life cycles, polypropylene (PP) and multiwall carbon nanotube filled PP (PP-MWCNT) plates with different thicknesses (from 0.25 mm to 2 mm) underwent accelerated weathering in a chamber that simulates solar irradiation and rainfall. The physicochemical changes of the plates depended on the radiation exposure, the plate thickness, and the presence of CNT fillers. Photodegradation increased with aging time, making the exposed surface more hydrophilic, decreasing the surface hardness and creating surface stress-cracks. Aged surface and cross-section showed crazing due to the polymer bond scission and the formation of carbonyls. The degradation was higher near the UV-exposed surface as the intensity of the radiation and oxygen diffusion decreased with increasing depth of the plates, resulting in an oxidation layer directly proportional to oxygen diffusion. Thus, sample thickness determines the kinetics of the degradation reaction and the transport of reactive species. Plastic fragments, which are less than 1 mm, and free CNTs were released from weathered MWCNT-PP. The concentrations of released NM that were estimated using ICP-MS, increased with prolonged aging time. Various toxicity tests, including reactive oxygen species generation and cell activity/viability, were performed on the released CNTs. The toxicity of the released fragments and CNTs to A594 adenocarcinomic human alveolar basal epithelial cells was observed. The released polymer fragments and CNTs did not show significant toxicity under the experimental conditions in this study. This study will help manufacturers, users of consumer products with nanocomposites and policymakers in the development of testing guidelines, predictive models, and risk assessments and risk based-formulations of NM exposure.

*Corresponding author: Sahle-Demessie.Endalkachew@epa.gov, Fax: +1-513-569-7677; Tel: +1-513-569-7739.

Keywords

1. Introduction

1.1 Background

Manufacturers of nanoparticle filled-polymer composites (polymer nanocomposites) are increasingly required for assurance of product lifetime, limiting the potential release of nanofillers from the polymer matrix during service life or when products are disposed of at the end-of-their use life. Polymer nanocomposites have attracted considerable interests in the auto industry, aerospace, packaging, sporting goods, electrical devices, and household goods. Due to inexpensiveness, high mechanical robustness, and high chemical resistance, polypropylene (PP) is widely used for various applications for packaging, food containers, laboratory equipment, water pipes, and anywhere resistance for heat, chemical, or electrical is required [1–3]. The international market research enterprise, Ceresana, reported that PP is the second worldwide most important polymer and 17.66 million tons was used for flexible packaging in 2016, but there is still a need to improve PP's property for providing higher mechanical robustness and chemical resistance along with multi-functions based on customers' demand (https://www.ceresana.com/en/about-us/). PP is filled and bonded with nanoparticles to produce materials with enhanced properties. Even though PP nanocomposites have been in existence for years, they have recently gained momentum in a wide range of mainstream commercial use.

Currently, various nanomaterials such as iron oxides, carbon black, silicon oxides, carbon nanofibers, and carbon nanotubes (CNTs) [4–8] are added as nanofillers in matrices of pristine polymers to improve their physicochemical properties (i.e., thermal, chemical, and mechanical stability, weight, and insulating property) for many applications. As reported, due to high thermal and chemical stability, high mechanical strength, and high thermal and electrical conductivity of CNTs, they have been widely used as a nanofiller, which resulted in the improvement of pristine polymers' physicochemical properties [9–13]. By adding CNTs, a half-time of the crystallization of PP significantly decreased while a rate of overall crystallization increased since CNTs played a role of a nucleation agent [14]. Prashantha et al. reported that the mechanical properties, including Young's modulus, tensile strength, yield stress, flexural rigidity, and Charpy impact resistance, were improved when CNTs were added up to 2 wt.% in PP but there was no properties' improvement compared to pristine PP beyond the optimal CNT content [12]. The thermal stability of CNT-PP composites was enhanced by the addition of CNTs [11]. Other studies reported the development of antimicrobial polymer composites using CNTs coatings [15, 16]. Bacteria, i.e., *Staphylococcus aureus* and *Escherichia coli*, were effectively killed since cell walls of bacteria were stabbed with CNTs immobilized in the composites, resulting in cell wall damages. Environmental aging of polymers is a complex process of oxidation, which leads to embrittlement and surface cracks, followed by chain scission and oxidation that leads to

discoloration. Despite a large amount of published work, there is no consensus on the mechanism and kinetics of polymer composites and the importance of thickness.

Kingston et. al. studied the degradation of five polymer nano-composites and charactering relating their release potential due to photodegradation and mechanical stresses across their life-cycle. The release of polymer nanocomposites was low in typical consumer applications. However, release occurs if the nanocomposite is exposed to conditions that degraded the bulk integrity of the polymer matrix [17, 18]. Meanwhile, there is a concern for environmental scientists regarding the release of nanomaterials from the polymer nanocomposites to the environment. Multiple studies have reported the toxicity of engineered nanomaterials even though CNTs provided advantages in the development of multi and high functional polymer materials [19–22]. Liu et al. summarized recent investigations about CNT toxicity [19]. The toxicity was caused by oxidative stress, inflammatory responses, malignant transformation, DNA damage and mutation, the formation of granulomas, and interstitial fibrosis. The toxicity was dependent on the physicochemical properties of CNTs, including shape, size, surface charge, impurity, and content of amorphous carbon in CNTs. Jafar et al. pointed out that CNTs easily enter into the human body due to their small size via inhalation, ingestion, and dermal exposure [20].

The release of nanoparticles and fibers from filled polymer-composites could be caused by mechanical actions, thermal and environmental degradation. The released nano-fillers could be transformed that alter their physio-chemical properties including their toxicity [23]. Due to their high stability, CNTs can stay in the environment and the human body for a long time and chronically provide adverse effects on the health of humans and animals. Aschberger et al. reported that the main route for CNT toxicity to human was chronic occupational inhalation, where a large number of CNTs was produced and their exposure was not controlled [21]. Straight multiwalled-CNTs (MWCNTs) showed a similar risk to human-like asbestos since they induced mesothelioma, but their effects depended on the adsorption and distribution in organs with different sensitivity to CNTs. Moreover, Du et al. reported that the toxicity of CNTs to the environment is significant and they are toxic to mammals and different species, i.e., fishes, microorganisms, and plants [22]. Due to their small size and chemical functional groups on their surface, they easily translocated through and accumulated in living cells, resulting in the death of cell and species, cytotoxicity, oxidative DNA damage, embryos immunological toxicity, inhibition of proliferation and growth of cell and species, bioaccumulation, and genotoxicity. Therefore, the release of carbon nanotubes embedded in polymer nanocomposites is of great interest regarding the safety of nanomaterials. Many consumer applications and industrial and environmental uses for plastic and nanocomposite as well as recycling require a thorough knowledge of polymer degradation and the toxicity of high concentration degradation products. Nanoparticles released from composites may be free-floating or embedded in polymer fragments. These released materials may have different physio-chemical and toxicity properties than their pristine forms. Pure nano-titania caused higher inflammatory effects in mice studies than nano-titania embedded in a paint matrix [24].

In this paper, we report the results of a systematic study of the aging of PP-MWCNT nanocomposite by weathering processes and the release of MWCNTs and micro-plastics

from the nanocomposites by weathering. For this study, MWCNTs were used to prepare PP-MWCNTs nanocomposites for the investigation of MWCNTs release from the nanocomposite. The release mechanism of MWCNTs to the environment were studied using the prepared PP-MWCNTs nanocomposites that were aged in a weathering chamber to simulate natural weather conditions and to accelerate the aging process.

The aged samples were characterized with scanning electron microscopy (SEM), contact angle measurement, digital microscopy, hardness measurement, X-ray diffraction (XRD) and Fourier-transform infrared spectroscopy (FTIR). Single particle- inductively coupled plasma mass spectrometry (ICP)-mass spectrometry (MS) (SP-ICP-MS) was used to quantify the released MWCNTs from the aged samples through the detection of metal nanoparticles embedded in the MWCNTs in samples. A short section of theoretical determination of environmental aging of PP-MWCNT nanocomposites has been provided in the Supporting Information. Weathered composites were showed and the released nanomaterials were detected using SP-ICP-MS through the detection of metal nanoparticles embedded in MWCNTs in samples [25–31]. SP-ICP-MS has been shown to provide a means to quantify the metal-content of SWCNTs [32, 33]. Metal catalysts used for the synthesis of CNTs or the metal impurities allows determination of SWCNT number concentrations. The metal content of the CNTs can be used as a proxy for determining the concentration of CNTs. However, there is little or no reported well-studied research on the use of such a method for determining the CNT-release from the polymer matrix.

The purpose of SP-ICP-MS was reported for detecting metal-containing nanoparticles in different matrices [34, 35]. The system can differentiate the particulate forms from the dissolved ion form of the elements that makes the technique a useful method for studying transformation on nanomaterials. A couple of metal catalysts, such as Ni, Fe, Co, and Mo are used for the synthesis of CNTs, the metal impurities allow determination of CNT concentrations. The metal content of the CNTs can be used as a proxy for determining the concentration of CNTs. However, there is little or no reported study on the use of such a method for determining the CNT-release from polymer matrix even though SP-ICP-MS provides an efficient way to characterize particle size and concentration for metallic nanoparticles [32, 36, 37]. In this study, the Sp-ICP-MS method was further expanded for detecting multi-walled carbon nanotube (MWCNT) released from polymer composite.

2. Experimental Section

2.1 Materials

The experimental methods include the preparation of the polymer nanocomposites with different thicknesses, the aging of the composites, the characterization of aged materials and the detection of the release of carbon nanotubes from aged composites.

2.2 Preparation of polypropylene and polypropylene-carbon nanotube composites plates

Polypropylene and PP-MWCNT composite plates were prepared using PP (Isotactic, average M_W ~250,000 and average M_N ~67,000) and NANOCYL™ NC7000 MWCNT (average diameter: 9.5 nm and average length: 1.5 μm) obtained from Sigma Aldrich and the

Nanocyl SA, respectively. All materials were used without any further treatment. The HAAKE™ PolyLab™ OS System ((Thermo scientific Haake Rheocord 90, Thermo Electron Corporation, Waltham, MA) was used for batch mixing melted polypropylene and PP-MWCNT for 30–60 min to obtain uniformly mixed PP-CNT materials before the mixtures were fed to the extruder to form large rolls of sheets of composite (See Supplemental Information Figure S1). The rheometer system simulates industrial processes in a pilot plant. The heating temperature was above 165 °C to effectively melt PP, and a MWCNTs content was 4 % (w/w) in the prepared PP-CNT materials. An extruder (Rheomex 102, USA) was used to prepare PP (PP0X) and PP-MWCNT (PP4X) films with three different thicknesses (Table 1) where X: thickness from 1 for thinnest to 3 thickest plates (See Supplemental Figure S2).

2.3   Weathering of films of PP and PP-MWCNT composites

Accelerated weathering of PP and PP-MWCNT composites was applied under a controlled and reproducible condition to achieve repeatability. A solar aging system equipped with a Xenon light lamp (Suntest XLS+, Atlas Material Testing Technology LLC) was used for direct setting and control of specimen chamber air temperature following ISO-4892–2/2013. Xenon-arc lamps give a much better spectral simulation to natural sunlight, although the Xenon-spectrum contains UV- wavelengths shorter than those found in solar radiation. More details of similar experimental protocols can be found in the literature [17, 18, 23, 24, 38, 39]. Others have used a similar experimental method [40]. The prepared films (5 cm × 5 cm) of PP and PP-MWCNT composites were immobilized on a stainless-steel mesh plate and placed in the weathering system. Thin plates of each group samples were taken out of the chamber at selected aging times of 756 h, 1512 h, 2268 h, and 3024 h, respectively. Solar irradiance at each sampling time was recorded and actual solar exposure time was calculated using annual solar radiant exposure data in subtropical regions (i.e., Florida, USA (6588 MJ/m^2)) from Atlas Material Testing Technology LLC (Ametek) (See Supplemental Fig. S3). For the weathering, a cycle of 120 min (i.e., 108 min sunshine and 12 min rain) was programmed and repeated until 3024 h of aging. The irradiance of solar light (wavelength: 200–800 nm) was 700 W/m^2 and the black substrate temperature was 65 °C. Humidity and heat in the weathering chamber during the process were monitored (Table 2 and 3).

2.4   Release of MWCNTs from aged PP-MWCNT composites

After weathering the PP-MWCNT plates for the total of 3024 h, a sample of ~100 mg of each plate was taken after a selected aging time and immersed in a 50 mL MilliQ-grade water (Resistivity: 18 MΩ·cm). The liquid samples, containing aged composites of 100 mg, were sonicated for one hour using a bath sonicator (Branson 2800, Branson Ultrasonics). After the sonication, the samples were used to study the release of MWCNTs from aged PP-MWCNT composites. Similar to many published studies [41], we considered the worst case of nanomaterial leaching from polymer-nanomaterial composites in the environment, we chose the sonication method in this study.

2.5 Analytical Methods

2.5.1. Sample Characterization—The changes of physicochemical properties of PP and PP-MWCNT composites during the weathering process were investigated. Surface morphology of unaged and aged samples was analyzed to determine changes in the physical properties using a Keyence VHX-600 digital microscope (Keyence Corp. of America) and a JEOL JSM-6490LV scanning electron microscope. Changes of samples' hardness by weathering were measured using a hardness testing machine (Akashi Corporation, Kanagawa, Japan). Contact angles of water on pristine and aged samples were measured with a drop shape analyzer (DSA25E, KRÜSS GmbH).

The changes in surface chemical functional groups by weathering was investigated with a Cary 660 FTIR spectrometer (Agilent Technologies) and a Cary 610 FTIR microscope (containing a 250 μm single-element, narrow-band Mercury Cadmium Telluride detector and a motorized sample stage) operating under Resolutions Pro 5.0 software. A constant flow of nitrogen was used to purge the system, limiting the contributions from carbon dioxide and atmospheric water vapor.

UV transmittance of pristine and aged samples was measured using a radiometer (Model IL1400A, International light, Inc.). XRD patterns of unaged and aged PP and PP-MWCNT plates samples were measured with a Panalytical (X'pert) 2θ diffractometer (Panalytical, Netherlands).

The release of MWCNTs from pristine and aged PP-CNT composites was investigated using liquid samples prepared with sonication. Particle size distributions of liquid samples were measured with a NanoBrook Omni dynamic light scattering (DLS) instrument (Brookhaven Instruments Co.).

2.5.2 Measuring Released Nanoparticles using ICP-MS, SP-ICP-MS and HR-TEM—The total mass of metal elements presented in the MWCNTs was determined by digesting 20 mg MWCNTs in 5 mL concentrated trace metal grade nitric acid, followed by ICP-MS analysis using EPA Method 3050B. The sample was digested on a hot block digester at 95 °C for 7 hrs, then added ultra-high purity water to bring the final volume to 10 mL. After centrifugation at 3000 G for 10 min, the supernatant was collected for ICP-MS analysis with appropriate dilution. A NexION 350D ICP-MS (PerkinElmer, Shelton, CT) was used for this analysis using KED mode to minimize interference. Based on the abundance and low interference from background elements, cobalt (Co) was selected as the target element to track MWCNT concentrations.

Further tests were performed to ascertain if Co nanoparticles are always embedded in MWCNTs or dissociated from MWCNTs. The MWCNTs were dispersed in 1% Triton-X solution by horn sonication procedure as descript above. The samples were passed through 0.22 μm nylon membrane filter (only the Co not embedded in MWCNTs pass through the filter). The transferred filtrate was acid digested at 90 °C for three hours in a hot block digester. The remaining solution was diluted to a known volume with ultrapure water and analyzed with ICP-MS (Table S1).

The released particles in aqueous samples obtained from the aged composites underwent similar sample preparation methods as the pure MWCNTs (Supplemental Figure S4). Weigh MWCNT 7000 accurately into a sampler tube; add 10 mL of 1% Triton-X aqueous solution to each tube; sonicate the samples for 30 mins at 4–6 Watts with a 3 mm diameter probe sonicator to disperse the sample; dilute the samples to appropriate concentrations; filter the diluted samples with a 0.22 (for Co not bond to MWCNT) or 1.5 μm (MWCNTs can pass through) size nylon membrane filter; further dilute the filtered standard to make different concentrations of standards for preparing calibration curves for SP-ICP-MS detection. The concentration of Triton-X in the final standard suspension was 0.0005% for SP-ICP-MS analysis. For the nanorelease suspension samples from aged composites, a small volume of concentrated Triton-X was added to make the Triton-X concentration same with the calibration standard (0.0005%), then processed through the same dispersion and filtration processes before SP-ICP-MS analysis. SP-ICP-MS analysis was performed to quantify released MWCNTs from aged PP-MWCNT samples. High-resolution transmission microscopy (HR-TEM) (JEM 2100, JEOL) was used to visualize individual MWCNTs, microsized PP (micro-PP plastic), and micro-PP plastic including MWCNTs in the liquid samples (Supplemental Figure S5 and S6).

2.5.3 Toxicity Determination of Aged-released Polypropylene and PP-MWCNT Composites

—Toxicity measurements were compared on paired samples of unaged and the most extended aging hours of polypropylene (PP01, PP02, and PP03) and PP-MWCNT composites (PP41, PP42, and PP43). Toxicity was determined using two different assays: Reactive Oxygen Species (ROS) formation assay and MTS Assay for cell viability and cell activity, as described previously [42]. Briefly, human alveolar epithelial cells (A549; CCL-185, ATCC) were cultured using Dulbecco's Modified Eagle Medium (DMEM, Gibco), supplemented with 10% FBS (Hi-Clone), 1% sodium pyruvate (Gibco), and 1% penicillin-streptomycin-neomycin (PSN, Gibco) and grown at 37 °C in 5% CO_2 atmosphere. Unaged and most aged PP and PP-MWCNT composites were suspended in cell culture media at a concentration of 12.5 mg/mL. The particle suspensions were sonicated as described above and then serially diluted to 2 mg/mL final concentration during exposure to cells. A control sample with media only was included in the sonication and toxicity tests.

ROS formation was determined using the dichlorofluorescein (DCF) assay. Conversion of H_2DCF (2′,7′-dichlorodihydrofluorescein, Molecular Probes) to fluorescent DCF signals the presence of ROS. For each test, 2×10^4 A549 cells were seeded per well of a 96 well plate in a volume of 200 μL and grown for 1 day, after which the media was replaced by 100 μL of 50 μM H2DCFDA in Hank's buffered salt solution (HBSS). After that, the cells were incubated for 60 min at 37 °C and 5% CO_2, followed by washing with prewarmed HBSS. Cells were then exposed to 100 μL of suspended solutions all samples. Peroxinitrite donor 3-morpholinosydnonimine (Sin-1, Sigma-Aldrich) was used as a positive control, as it generates both superoxide anions and nitric oxide that spontaneously form peroxynitrite, a potent oxidant. Fluorescent intensities were measured after 2 h using a fluorescent microplate reader (Molecular Devices) at an excitation wavelength of 485 nm and an emission wavelength of 528 nm. Fluorescence values were blank-corrected and normalized.

The MTS Assay, measuring cell viability and cell activity, was determined using the CellTiter 96 AQueous One solution (Promega) containing 3-(4,5-dimethylthiazol-2-yl)-5-(3-carboxymethoxyphenyl)-2-(4-sulfophenyl)-2H–tetrazolium inner salt [MTS] as the tetrazolium compound and an electron coupling reagent (phenazine ethosulfate; PES). To perform the assay, 8×10^3 A549 cells seeded in 200 μL of complete cell culture medium per well of a 96 well plate and grown for 1 day. Afterward, cells were exposed to 200 μL of suspended solutions of all samples or the positive control $CdSO_4$ (100 μM) for 24 h, at which point the medium was replaced by 120 μL of MTS working solution. The plate was incubated for 60 min at 37 °C and 5% CO_2 before the optical density was measured at 490 nm in a microplate reader (Molecular Devices).

3. Results and discussion

3.1 Changes of Mechanical Property of PP-MWCNT Composites by Weathering

Studying the effects of the thickness distribution of photooxidation offers a method to establish the effects of diffusion control kinetics of photoaging. Optical photomicrographs of unfilled and MWCNT filled PP at selected exposure times (Figure 1a). Figure 1b shows 3D images and surface roughness of at selected weathering times ranging from pristine to 3024 h. As images show in figure 1 the unfilled PP thin plates, PP01 and PP02, were crushed after 1512 h and 2268 h, respectively, long before planned 3024 h. The aging process evident in these samples as they became very brittle due to oxidation and crystallization during the weathering process creating structural failures. The thickest polypropylene sample, PP03, and PP-MWCNT samples were not broken after 3024 h of weathering, indicating that the added MWCNTs reinforced the mechanical and thermal stability of polypropylene. As seen in Figure 1b, weathering caused surface oxidation and erosion that resulted in the formation of cracks on the surface of the samples and increased the surface roughness of aged samples significantly (See supplemental Figure S7). Moreover, a measured hardness of most samples dramatically decreased after 756 h of weathering except for PP43, the thickest PP-MWCNT composite sample (Supplemental Table S1). Most aged PP samples were shattered when an indenter touched samples, while all PP-MWCNT composites were not ruined during the hardness measurement (Supplemental Figure S8). Even though the measured hardness were negative values, it shows that aged polymer composites became brittle due to oxidation and crystallization of samples during the weathering process. Previous studies reported that polymers became brittle due to a decrease of molecular weight in the polymers' surface by oxidation during aging processes. Once the molecular weight decreased to a certain critical level of each type of polymer or composite by photooxidation, polymers lost resistance to internal stress, resulting in the formation of cracks and loss of elasticity, became brittle [43–46].

Surface scanning electron micrographs of surface and cross-sectional images of polypropylene (PP01, PPO2, PP03) and PP-MWCNT (PP41, PP42, PP43) showing surface cracks the width of the cracks (Figure 2). Earlier studies have indicated that crazes evolve from micro-deformation processes in localized regions about 30 nm in diameter. As the irradiation increased, the deformation region develops, further localized deformation was induced. The growth and coalescence of such deformed nuclei create a narrow plastic zone

that forms voided structure. These voided precursors are considered the precursor of the fibrillated craze structure that ultimately leads to failure [47].

3.2 Changes of Surface Morphology of PP-MWCNT Composites by Weathering

For investigating the morphological changes of PP-MWCNT composites during the weathering process, the surface and cross-section of raw and aged samples were observed using SEM. Figure 2 and Figure S7 show SEM images of pristine and aged PP-MWCNT composites (i.e., PP01, PP02, PP03, PP41, PP42, and PP43). As seen the figures, numbers of micro-cracks on the surface of the nanocomposites increased, and the surface became very rough due to the formation of cracks. Moreover, as seen in a schematic in Figure 2, the width and depth of cracks formed on the surface of aged samples became broader and more profound. It seems that the surface was eroded due to surface oxidation and a washing process during the weathering process. Previous studies by Kumar et al. reported the formation of micro-cracks and matrix erosion in epoxy-carbon nanofiber nanocomposites by UV photooxidation and water condensation [48].

Due to the evaporation of volatile compounds and moisture in the polymer matrix by UV irradiation and breakage of polymer structure by photooxidation, the surface of the polymer was eroded and there was a loss of microplastics and nanofibers from the matrix, resulting in the formation of cracks, rough surface, and void in the matrix of the polymer nanocomposites. Since water was sprayed on the surface of the aged polymer composites during the weathering process, weakened parts (i.e., oxidized parts) of the aged samples could be easily washed away and water-soluble compounds formed by the degradation process could be removed from the aged polymer nanocomposites. Audouin et al. reported that there are two domains in polymer matrix, depending on thickness or molecular weight of polymer samples: one is Domain I, where the degradation kinetics is not dependent on diffusion and the other is Domain II, where diffusion is an important parameter for the degradation kinetics [49]. Within the domains, oxidation, hydrolysis, and ozonolysis are involved in the degradation of polymers during aging processes. In Domain I, the degradation occurs uniformly in the polymer matrix due to low molecular weight or small thickness of polymers, but the degradation is very non-uniform at the surface and in the matrix of polymers since it takes longer time for oxidant diffusion into thick polymer matrix in case of Domain II (i.e., thick sample). In most cases of polymer aging, small and shallow cracks form at the beginning of the aging process due to surface oxidation and erosion.

The cracks formed became wider and deeper over aging times due to the oxidation of inside of the polymer matrix, resulting from increased oxidant permeability into the polymer. Figure 2 and Figures S5 to S7 clearly show the formation of cracks and their widening and deepening on the surface and inside of polymer composites along with the formation of micro-cracks in the polymer matrix during weathering aging, which are in good agreement with the previous studies have reported that cracks started forming on the surface of PP due to photooxidation and the photooxidation thickness of polymers was proportional to aging times and temperatures [43, 48–51].

3.3 Changes in Surface Hydrophobicity of aged PP and PP-MWCNT composite

In addition to the changes of surface chemistry by weathering, the hydrophilicity of polymers' surface was observed by measuring contact angles of aged samples. As seen in Figure 3, there are no effects of the addition of MWCNTs in PP on contact angles since contact angles for all samples are very similar around 94 to 100°. Contract angles for polypropylenes without carbon nanotube significantly decreased by 70 percent to around 30° except for the thinnest PP plates, indicating the surface of samples were damaged and oxidized by photooxidation, chemical oxidation, and physical erosion. Since functional groups formed by the oxidation during the weathering process, the surface of aged polypropylene samples without MWCNTs became more hydrophilic. Since the photooxidation and chemical oxidation occurred on the surface of the samples, the hydrophilicity of the thickest PP sample did not change, significantly. However, for aged PP-MWCNT samples, their contact angles increased over aging times and then, decreased.

At the beginning of the weathering process, UV photooxidation and chemical oxidation started from the surface of the samples and then, hydrophobic MWCNTs in the polymer matrix gradually appeared on the surface of the samples, increasing of the contact angles. When the samples exposed to solar light and moisture for a long time, PP and exposed MWCNT on the surface of PP oxidized together during the weathering process, which resulted in a small decrease of contact angles. Interestingly, their contact angles were still larger than their initial contact angles, but broader and deeper cracks formed on their surface compared to aged PP samples (Figure S7(b)). After 1500 h of aging the contact angle of PP-MWCNT increased by ~30 °, which could be due to the degradation of polymer surfaced exposing more CNTs on the surface of the aged plates (Figure 3). It seems that embedded carbon nanotubes not only absorbed more illumination due to their color but also provided holding forces to the polymer matrix, partially. Due to the part provided partial holding forces in the polymer matrix, different stress was involved during expansion and contraction of the samples during the weathering process. Other studies reported UV aged polymers became more hydrophilic due to the formation of functional groups by photooxidation [52–54]. The changes in surface hardness show that at the end of the induction period of the oxidation of PP and PP-MWCNT (Figure S8).

3.4 Change in the light transparency of Polypropylene

The progress of PP degradation of with time can be measured based on the transparency of plate for light. UV radiation in oxidative environment promotes chain scission with the formation of free radicals. PP and some other polyolefins should be transparent to sunlight, i.e., to wavelength > 290 nm. However, PP exposure to sunlight in the presence of air-humidity leads to the photooxidation of PP modifying the microstructure and physicochemical properties as manifested by embrittlement and craze formation, and the absorption of photons as shown in Figure 4. Weathering is a complex process involving multiple factors such as temperature, humidity, UV radiation, and their interactions. The behavior of light UV spectrophotometric measurements allows, a semi-quantitative relation between the screening effect of polyenes and the thickness effects on weathering. Changes of light transparency profiles across the three plates during photoaging in the accelerated aging chamber are based on $I = I_o + a * \exp(-b * t)$, where a is a constant, b is irradiation of

the light intensity and t is the exposure time. Regression analysis was used to model light transmission data as an empirical approach [55]. The presence of tertiary carbon in the structure of PP makes it sensitive to environmental aging. This is because disruption of tertiary carbon may form macroradicals by $P^{\bullet}$ that interact with oxygen to makes peroxides. The main transformation of the macromolecular chain consists of the formation of carbonyl and vinyl groups [56]. As the weathering of PP, PP-MWCNT increased light-absorbing groups implicated in photo-oxidation hydroperoxide, peroxide, methyl ketone end groups and oxygen-hydrocarbons that is discussed in the next section.

3.5   Changes of Surface Chemistry of PP-MWCNT Composites by Weathering

Weathering is sufficient to cause the breakdown of polymeric C–C bonds or form carbonyls because of degradation. The resulting smaller fragments do not contribute effectively to the mechanical properties and the PP becomes brittle limiting it use-life and causing product failure. Fourier transform infrared spectrometer was used to measure the infrared absorption spectrum of the post-exposure PP and PP-MWCNT sample plates (thickness 0.25 to 2 mm) in the range from 4000 cm^{-1} to 1600 cm^{-1} on absorption mode at a typical average of 30 scans.

The permeability of atmospheric oxygen is low in PP, and hence the diffusion of oxygen in thick plates determine the extent of oxidation limit it to the most superficial layers. FTIR studies were conducted on the exposed surface of the test plates. The surface chemical profiles of fresh and solar aged unfilled and MWCNT polypropylene plates were monitored following the procedures described in the experimental section. Figures 5(a–f) and 6(a–f) show the results of FTIR analysis for aged PP and PP-MWCNT composites, respectively. In all raw PP and PP-MWCNT composites, typical peaks of antisymmetric stretching -CH$_3$ methyl group, symmetric stretching -CH$_3$-, antisymmetric stretching -CH$_2$- methylene group, and symmetric stretching -CH$_2$- were observed at 2970 cm^{-1}, 2910 cm^{-1}, 2870 cm^{-1}, and 2840 cm^{-1}, respectively. Peaks, corresponding to -CH$_2$- bending and -CH$_3$ bending, were detected at 1460 cm^{-1} and 1370 cm^{-1}, respectively in the raw samples as reported in previous studies [57–59]. Since MWCNTs added in the PP-MWCNT composites were not functionalized, there are no differences of FTIR peaks between raw PP and raw PP-MWCNT composites.

During the weathering process, the height of the IR absorption peaks increased from 1850 cm^{-1} to 1540 cm^{-1}, corresponding to carbonyl groups and carboxylate bands, and a peak from 3600 cm^{-1} to 3000 cm^{-1}, corresponding to hydrogen-bonded hydroperoxides, was observed while peaks from 2970 cm^{-1} to 2840 cm^{-1} decreased [57–60]. It indicates the surface of PP and PP-MWCNT composites was oxidized due to photooxidation and chemical oxidation by O_3 formed in the weathering chamber. Due to solar irradiation during the aging, ozone was formed and was involved in the polymer degradation of water bubbled with air taken from the weathering chamber during the aging process. Interestingly, a broad peak from 2150 cm^{-1} to 2020 cm^{-1}, corresponding to carbonyls, was observed.[61] It might be due to the presence of MWCNTs, providing high pure carbon in the polymer matrix, which was oxidized during the weathering process. The carbonyl index (CI) was calculated

from the absorbances at around 1715 cm^{-1} (peak of carboxyl group produced by photooxidation) and 2020 cm^{-1} (peak of methylene group (standard)), according to:

$$CI = {A_{1715}} \big/ {A_{2020}} \qquad (1)$$

The photooxidation degradation of PP involves the formation of chain end carboxylic acids on the normal methylene groups and the vinylidene defects. The carboxylic acid groups absorb at 1715 cm^{-1}. Photodegradation usually starts at the surface with visible cracks and discoloration. In theory, olefins such as polypropylene (PP) are stable when exposed to sunlight, because both C-C and C-H bonds do not absorb UV radiation from the sun. However, there are often contaminations present which can initiate photodegradation resulting in surface cracking and loss of mechanical properties. Several mechanisms contribute to photodegradation. If free radicals are directly produced by UV radiation, they could cause chain scission, crosslinking, and secondary oxidation. Another mechanism of photooxidation includes the photochemical production of electronically excited oxygen. In this case, degradation takes place by direct oxidation, for example, by reaction with allylic hydrogen which then could undergo chain scission with formation of terminal ketone groups. Another contributor to photo degradation is ketone photolysis which proceeds via Norrish reaction, where ketones are formed by either thermolysis or photolysis of hydro peroxides. If these groups are exposed to light, they undergo chain scission via Norish I or II reaction. Thus, Vinyl group undergo Norrish type II process to form ketonic groups that contribute to cross-linking and absorb at 1640 and 909 cm^{-1} [62]. The carbonyl index increased at almost a constant rate without any induction period (Supplemental Figures S9 (a) and (b)), which could be because that carbonyl build-up is not auto-accelerated to indicate that oxidation reaches a stationary state rapidly [63].

3.6 Thickness distribution effect of degradation

Environmental stress cracking is one of the common cause of polymer failure that could result in the release of fragments and embedded additives. Micro-crack formation increases absorption of moisture than unaged PP, exposing the wet composite to further degradation. Figure 7 shows a schematics representation of the surfaced aging, formation of cracks. The SEM image of the surface and cross-sections views of aged PP and PP-MWCNT shows the degradation within the sample thickness that is controlled by the oxygen diffusion on kinetics (Supplemental Figure S10). A superficial layer rich in oxidation product was showing photodegradation including embrittlement and loss of transparency.

For diffusion-controlled aging, embrittlement depends on superficial degradation. Thus, unfilled thin PP samples showed more "sensitivity' to rupture. [64]. Polypropylene is a polycrystalline material where the crystal structures form randomly distributed microcrystalline domains. Figure S11 shows the XRD diagrams for unaged and aged PP showing characteristic peaks of crystal planes (110, 040, 130, and 110) and suggests the aging process did not change the crystal form. The diffraction pattern of PP-MWCNT composite includes the 002 planes for CNT at 2q ~ 26° (Figure S12). Diffusion peaks were becoming wider, indicating a decrease in the crystal size. However, X-ray diffraction

patterns of PP and PP-MWCNT did not show weathering affects the loss of crystallinity, defects, or peak broadening.

3.7 Release of MWCNTs from the aged PP-MWCNT composites

Increased weathering caused matrix photodegradation and release of fragments. Although the release of polymer and nanofillers from photodegraded products were previously studied, the effects of plate thickness and metal ions embedded in CNTs at different irradiated polymer matrix were not investigated rigors (Supplemental Figure S13). The release of micro-fragments and MWCNTs from aged PP-MWCNTs was studied using dynamic light scattering (DLS) analysis of the suspension and TEM. Figures 8 shows that not only microplastics containing MWCNTs ranging from few nanometers to several micrometers were released from aged PP-MWCNT composites, but also individual MWCNTs with different length from 50 nm to few hundred nanometers were released. Sizes of both microplastics and MWCNTs were very different due to random aging.

In addition to the TEM analysis for nano-release study, DLS was used to measure the particle size distribution of released materials from aged PP-MWCNT composites. As seen in Figure 9 (a to 9(d), particle size distribution of released samples decreased from several hundred nanometers to few nanometers after filtering released samples using 0.45 μm syringe filters (Whatman™ GD/X PVDF Syringe Filters), indicating both microplastics and carbon nanotubes are released together and the presence of nanomaterials in the samples was hidden by microplastic particles (Supplemental S14). The shapes of the profiles and the average diameter of the DLS curves show the overall behavior of the polymer results from photodegradation changes with time. After filtering, we effectively observed the presence of release nanomaterials from aged composites. The released nanoparticles were detected in all aged PP-MWCNT composites. Although some of the aged samples (PP43) showed detected nanoparticles in the sample aged for 756 h, there was little released CNT detected overextended aging. The hollow core structure of the released CNT closely similar to the original CNT added to PP as a filler (Figure 8 and Figure S14). It seems the oxidation occurred at the surface of PP43 sample and a little MWCNTs appeared at the early stage of aging only. Then, the exposed MWCNTs on the surface of PP43 were washed out during the spraying time, and no further oxidation occurred due to samples' thickness even though PP43 sample was aged for longer times.

3.8 Quantification of released MWCNTs from aged PP-MWCNTs composites by SP-ICP-MS analysis

One approach of quantifying the release of CNT as the result of abrasion of polymer nanocomposite was by pre-labeling MWCNT with lead ion and analyzing acid digested released particles using ICP-MS. The method allowed the quantification of MWCNT that free released and protruding [65]. We used SP-ICP-MS, an emerging technology for nanoparticle analysis that can quantitatively detect particles at an ultra-low concentration in the complex sample matrix. Though the method cannot detect carbon nanotubes (CNTs) directly, it has been applied for single-walled CNP detection through monitoring the embedded metals in the CNTs [33]. In this study, we have used SP-ICP-MS method to detect embedded Co in MWCNTs for quantitatively determination of MWCNTs release

from aged PP-MWCNTs. The total MWCNT concentration is the sum of "dissolved" (0.22 μm membrane filtered, including CoNPs with a size smaller than the size detection limit, and dissolved Co) and particle concentration (1.5 μm membrane filtered, include Co-MWCNTs and CoNPs in microplastics) (Supplemental Figure S4). Figures 9 shows a hydrodynamic diameter of the released fragments decreased with the time of aging. MWCNTs release pattern affected by the thickness of the PP-MWCNT composites used for the tests (Supplemental S16). The release increased quickly starting at an early aging time for the thin composite (PP41) without acceleration at the late aging time. The release increasing rate accelerated at a longer aging time for the thicker PP-MWCNTs (PP43). As the aging time increased most of the Co was present as nanoparticle (Co-NP) dissociated from MWCNTs in the polymer composite.

3.9 Toxicity of released microplastics and MWCNTs from aged PP-MWCNTs composites

Saber et al. conducted a comparative toxicity study involving dust generated from the mechanical abrasion of epoxy and MWCNT-epoxy nanocomposites. Epoxy dust with and without CNT can get deposed in pulmonary tissue induced inflammation and DNA damage in lung tissue. However, the researchers did not observer added effects due to the CNT filler in the epoxies for any of the pulmonary endpoints [39]. In this study, toxicity assessments were done of paired samples of no aging (0 h) to maximum aging on both the polypropylene samples and PP-MWCNTs. Formation of reactive oxygen species (ROS) in cells exposed to toxins and the effects on cell activity and viability of cells are common ways of measuring toxicity [42, 66–68]. With inhalation being a primary route for degraded nanoparticles, the toxicity of the non-aged and aged samples was tested on A549 alveolar epithelial cells. The production of intracellular ROS was measured on all samples, using Sin-1 as a positive control, which generates both superoxide ions and nitric oxide, spontaneously forming peroxynitrite, a potent oxidant. As shown in Figure 11a, neither the aged or non-aged samples produced significant levels of ROS, suggesting that the degradation does not produce radical oxides as toxins. Further toxicity testing was done using the MTS assay, which assesses cell activity and viability. MTS is a compound that is bioreduced by cells into formazan, a colored product that can be detected by optical density. In this study, cells were exposed to a total of 24 h to the samples and compared to non-exposed cells (negative control) (Figure 11b). The assay indicated that while the positive control, $CdSO_4$, reduced cell activity, none of the paired aged and non-aged samples had any significant effects on cell activity compared to the negative control. Although there have been studies analyzing MWCNT composites [4, 69, 70], there are no studies to date, evaluating the toxicity of polypropylene and PP-MWCNT composites. Although the non-aged and aged samples in this study did not produce degraded products that cause toxicity, changes to the functional groups or other surface properties of the same nanoparticles can affect toxicity levels.

4. Conclusions

PP was exposed under the water spray condition by using Xenon arc lamp. We evaluated the synergistic effect of light and moisture using the quantification technique of degradation. In this study, PP and PP-MWCNT composites were aged in an accelerated weathering chamber that simulates cycles of solar irradiation and rainfall. Aged plates were taken out at selected

times to evaluate the effects of weathering. The changes in physicochemical properties modulated by sample thicknesses and the added MWCNTs during the weathering process were investigated. The surface oxidation of polypropylene plates was found to result in extensive surface restructuring. This restructuring was detected by craze and crack formation, changes in hydrophobicity, and in surface infrared spectra, as measured by attenuated total reflection spectroscopy, and by electron microscopy.

The results revealed that (1) surface oxidation increased in crystallinity causing the surface to become brittle during the weathering process. This loose of elasticity resulted in a craze and cracks formation and further degradation of the thinner samples. Oxidation penetrated selectively into the polymer structure. Cracks were reduced by the presence of CNT at high content; (2) composites containing CNT showed less loss of surface hardness, fewer cracks, and higher hydrophobicity on weathered surface than other groups, confirming its functions of stabilization and antioxidation; (3) The 1775 cm−1/2879 cm−1 absorbance ratio of the FTIR plat surfaces increased steadily during ultraviolet degradation and was due to the increase in helical ordering which resulted from backbone scission during irradiation. (4) When the aged PP, and PP-MWCNT were placed in sonication water-bath fragments of polymer, CNT and metals were released. The release of MWCNT and composite-fragments that were determined using a high-resolution transmission electron microscopy (HR-TEM), and dynamic light scattering (DLS) showed that there was an increase in the volume of released materials and a decrease in the particles size of the released fragments with aging. The metal ions in released MWCNTs were quantified with a single particle-ICP analysis. (5) Lastly, the toxicity of released particles was investigated.

The released PP fragments and CNT did not show significant toxicity. Our combined results demonstrated the little toxicity of the released MWCNT-embedded PP to A594 adenocarcinomic human alveolar basal epithelial cells. This study which will help with future risk based-formulations of exposure to engineered nanoparticles and it could provide beneficial information to researchers and decision-makers in the field of environmental engineering for understanding weathering of polymers, nano released from polymer-nanomaterial composites, and their toxicity. This kind of model of photooxidation would be advantageously applied to other nanopolymer composites for which the absorbance behavior and other parameters are identified and their photochemical characteristics measurable with accuracy.

Supplementary Material

Refer to Web version on PubMed Central for supplementary material.

Acknowledgement

5. References

1. de Dicastillo CL, et al., Immobilization of green tea extract on polypropylene films to control the antioxidant activity in food packaging. Food research international, 2013 53(1): p. 522–528.

2. Lepot N, et al., Influence of incorporation of ZnO nanoparticles and biaxial orientation on mechanical and oxygen barrier properties of polypropylene films for food packaging applications. Journal of applied polymer science, 2011 120(3): p. 1616–1623.

3. De Volder MF, et al., Carbon nanotubes: present and future commercial applications. science, 2013 339(6119): p. 535–539. [PubMed: 23372006]

4. Zhu J, Wei S, and Guo Z, Magnetic Polypropylene Nanocomposites Reinforced with In-situ Fabricated Iron Oxide Nanoparticles. MRS Online Proceedings Library Archive, 2011 1312.

5. Rong MZ, et al., Analysis of the interfacial interactions in polypropylene/silica nanocomposites. Polymer International, 2004 53(2): p. 176–183.

6. Hammel E, et al., Carbon nanofibers for composite applications. Carbon, 2004 42(5–6): p. 1153–1158.

7. Schawe JE, Pötschke P, and Alig I, Nucleation efficiency of fillers in polymer crystallization studied by fast scanning calorimetry: Carbon nanotubes in polypropylene. Polymer, 2017 116: p. 160–172.

8. Kanbur Y and Küçükyavuz Z, Electrical and mechanical properties of polypropylene/carbon black composites. Journal of Reinforced Plastics and Composites, 2009 28(18): p. 2251–2260.

9. Chen W, et al., Enhanced mechanical properties and morphological characterizations of poly (vinyl alcohol)–carbon nanotube composite films. Applied Surface Science, 2005 252(5): p. 1404–1409.

10. Kim JY, Han SI, and Hong S, Effect of modified carbon nanotube on the properties of aromatic polyester nanocomposites. Polymer, 2008 49(15): p. 3335–3345.

11. Manchado ML, et al., Thermal and mechanical properties of single-walled carbon nanotubes–polypropylene composites prepared by melt processing. Carbon, 2005 43(7): p. 1499–1505.

12. Prashantha K, et al., Masterbatch-based multi-walled carbon nanotube filled polypropylene nanocomposites: Assessment of rheological and mechanical properties. Composites science and technology, 2009 69(11–12): p. 1756–1763.

13. Zeng H, et al., In situ polymerization approach to multiwalled carbon nanotubes-reinforced nylon 1010 composites: mechanical properties and crystallization behavior. Polymer, 2006 47(1): p. 113–122.

14. Valentini L, et al., Effects of carbon nanotubes on the crystallization behavior of polypropylene. Polymer Engineering & Science, 2004 44(2): p. 303–311.

15. Kang S, et al., Single-walled carbon nanotubes exhibit strong antimicrobial activity. Langmuir, 2007 23(17): p. 8670–8673. [PubMed: 17658863]

16. Pangule RC, et al., Antistaphylococcal nanocomposite films based on enzyme– nanotube conjugates. ACS nano, 2010 4(7): p. 3993–4000. [PubMed: 20604574]

17. Kingston C, et al., Release characteristics of selected carbon nanotube polymer composites. Carbon, 2014 68: p. 33–57.

18. Harper S, et al. Measuring nanomaterial release from carbon nanotube composites: review of the state of the science in Journal of Physics: Conference Series. 2015 IOP Publishing.

19. Liu Y, et al., Understanding the toxicity of carbon nanotubes. Accounts of chemical research, 2012 46(3): p. 702–713. [PubMed: 22999420]

20. Jafar A, Alshatti Y, and Ahmad A, Carbon nanotube toxicity: The smallest biggest debate in medical care. Cogent Medicine, 2016 3(1): p. 1217970.

21. Aschberger K, et al., Review of carbon nanotubes toxicity and exposure—Appraisal of human health risk assessment based on open literature. Critical reviews in toxicology, 2010 40(9): p. 759–790. [PubMed: 20860524]

22. Du J, et al., Understanding the toxicity of carbon nanotubes in the environment is crucial to the control of nanomaterials in producing and processing and the assessment of health risk for human: a review. Environmental Toxicology and Pharmacology, 2013 36(2): p. 451–462. [PubMed: 23770455]

23. Wang J, Schlagenhauf L, and Setyan A, Transformation of the released asbestos, carbon fibers and carbon nanotubes from composite materials and the changes of their potential health impacts. Journal of nanobiotechnology, 2017 15(1): p. 15. [PubMed: 28219381]

24. Saber AT, et al., Nanotitanium dioxide toxicity in mouse lung is reduced in sanding dust from paint. Particle and Fibre Toxicology, 2012 9(1): p. 4. [PubMed: 22300483]

25. Hadioui M, Leclerc S, and Wilkinson KJ, Multimethod quantification of Ag+ release from nanosilver. Talanta, 2013 105: p. 15–19. [PubMed: 23597981]

26. Dan Y, et al., Characterization of gold nanoparticle uptake by tomato plants using enzymatic extraction followed by single-particle inductively coupled plasma–mass spectrometry analysis. Environmental science & technology, 2015 49(5): p. 3007–3014. [PubMed: 25633589]

27. Dan Y, et al., Single particle ICP-MS method development for the determination of plant uptake and accumulation of CeO2 nanoparticles. Analytical and bioanalytical chemistry, 2016 408(19): p. 5157–5167. [PubMed: 27129977]

28. Dan Y, et al., Rapid analysis of titanium dioxide nanoparticles in sunscreens using single particle inductively coupled plasma–mass spectrometry. Microchemical Journal, 2015 122: p. 119–126.

29. Donovan AR, et al., Single particle ICP-MS characterization of titanium dioxide, silver, and gold nanoparticles during drinking water treatment. Chemosphere, 2016 144: p. 148–153. [PubMed: 26347937]

30. Donovan AR, et al., Detection of zinc oxide and cerium dioxide nanoparticles during drinking water treatment by rapid single particle ICP-MS methods. Analytical and bioanalytical chemistry, 2016 408(19): p. 5137–5145. [PubMed: 26960902]

31. Donovan AR, et al., Fate of nanoparticles during alum and ferric coagulation monitored using single particle ICP-MS. Chemosphere, 2018 195: p. 531–541. [PubMed: 29277033]

32. Pace HE, et al., Determining transport efficiency for the purpose of counting and sizing nanoparticles via single particle inductively coupled plasma mass spectrometry. Analytical chemistry, 2011 83(24): p. 9361–9369. [PubMed: 22074486]

33. Reed RB, et al., Detection of single walled carbon nanotubes by monitoring embedded metals. Environmental Science: Processes & Impacts, 2013 15(1): p. 204–213. [PubMed: 24592437]

34. Wang J, et al., Analysis of single-walled carbon nanotubes using spICP-MS with microsecond dwell time. NanoImpact, 2016 1: p. 65–72.

35. Laborda F, et al., Selective identification, characterization and determination of dissolved silver (I) and silver nanoparticles based on single particle detection by inductively coupled plasma mass spectrometry. Journal of Analytical Atomic Spectrometry, 2011 26(7): p. 1362–1371.

36. Domingos RF, et al., Characterizing manufactured nanoparticles in the environment: multimethod determination of particle sizes. Environmental science & technology, 2009 43(19): p. 7277–7284. [PubMed: 19848134]

37. Degueldre C and Favarger P-Y, Colloid analysis by single particle inductively coupled plasma-mass spectroscopy: a feasibility study. Colloids and Surfaces A: Physicochemical and Engineering Aspects, 2003 217(1–3): p. 137–142.

38. Gomez V, et al., Comparison of dust release from epoxy and paint nanocomposites and conventional products during sanding and sawing. Annals of occupational hygiene, 2014 58(8): p. 983–994. [PubMed: 25030708]

39. Saber AT, et al., Epoxy composite dusts with and without carbon nanotubes cause similar pulmonary responses, but differences in liver histology in mice following pulmonary deposition. Particle and fibre toxicology, 2015 13(1): p. 37.

40. Wohlleben W and Neubauer N, Quantitative rates of release from weathered nanocomposites are determined across 5 orders of magnitude by the matrix, modulated by the embedded nanomaterial. NanoImpact, 2016 1: p. 39–45.

41. Wohlleben W, et al., NanoRelease: Pilot interlaboratory comparison of a weathering protocol applied to resilient and labile polymers with and without embedded carbon nanotubes. Carbon, 2017 113: p. 346–360. [PubMed: 30147114]

42. Han C, et al., Evaluating Weathering of Food Packaging Polyethylene-Nano-clay Composites: Release of Nanoparticles and their Impacts. NanoImpact, 2018 9: p. 61–71. [PubMed: 29226269]

43. Girois S, et al., Oxidation thickness profiles during photooxidation of non-photostabilized polypropylene. Polymer degradation and stability, 1997 56(2): p. 169–177.

44. Fayolle B, Audouin L, and Verdu J, Oxidation induced embrittlement in polypropylene—a tensile testing study. Polymer Degradation and Stability, 2000 70(3): p. 333–340.

45. Fayolle B, Audouin L, and Verdu J, A critical molar mass separating the ductile and brittle regimes as revealed by thermal oxidation in polypropylene. Polymer, 2004 45(12): p. 4323–4330.

46. Fayolle B, et al., Mechanism of degradation induced embrittlement in polyethylene. Polymer Degradation and Stability, 2007 92(2): p. 231–238.

47. Arnold J, Environmental stress crack initiation in glassy polymers. Trends in polymer science, 1996 12(4): p. 403–408.

48. Kumar BG, Singh RP, and Nakamura T, Degradation of carbon fiber-reinforced epoxy composites by ultraviolet radiation and condensation. Journal of Composite materials, 2002 36(24): p. 2713–2733.

49. Audouin L, et al., Role of oxygen diffusion in polymer ageing: kinetic and mechanical aspects. Journal of Materials science, 1994 29(3): p. 569–583.

50. Awaja F, et al., Cracks, microcracks and fracture in polymer structures: Formation, detection, autonomic repair. Progress in Materials Science, 2016 83: p. 536–573.

51. Chowdhury M, et al., Intrinsic stresses in thin glassy polymer films revealed by crack formation. Macromolecules, 2016 49(23): p. 9060–9067.

52. You J, et al., Direct photo-patterning on anthracene containing polymer for guiding stem cell adhesion. Biomaterials research, 2016 20(1): p. 26. [PubMed: 27489725]

53. Suresh B, et al., Mechanical and surface properties of low-density polyethylene film modified by photo-oxidation. Polymer journal, 2011 43(4): p. 398.

54. Xu Q, et al., Reactive oxygen species (ROS) responsive polymers for biomedical applications. Macromolecular bioscience, 2016 16(5): p. 635–646. [PubMed: 26891447]

55. Maxwell A, et al., Review of accelerated ageing methods and lifetime prediction techniques for polymeric materials. NPL Report DEPC MPR, 2005 16: p. 22.

56. Feldman D, Polymer weathering: photo-oxidation. Journal of Polymers and the Environment, 2002 10(4): p. 163–173.

57. Barbeş L, Rădulescu C, and Stihi C, ATR-FTIR spectrometry characterisation of polymeric materials. Romanian Reports in Physics, 2014 66(3): p. 765–777.

58. Silva RA, Silva P, and Carvalho M. Degradation Studies of Some Polymeric Biomaterials: Polypropylene (PP) and Polyvinylidene Difluoride (PVDF) in Materials science forum. 2007 Trans Tech Publ.

59. Zaiqing W, Xingzhou H, and Deyan S, The FTIR studies of photo-oxidative degradation of polypropylene. 感 光 科, 1988 6(3): p. 285–288.

60. Mylläri V, Ruoko TP, and Syrjälä S, A comparison of rheology and FTIR in the study of polypropylene and polystyrene photodegradation. Journal of Applied Polymer Science, 2015 132(28).

61. Kondarides DI, Chafik T, and Verykios XE, Catalytic reduction of NO by CO over rhodium catalysts: 3. The role of surface isocyanate species. Journal of Catalysis, 2000 193(2): p. 303–307.

62. Arnaud R, Moisan JY, and Lemaire J, Primary hydroperoxidation in low-density polyethylene. Macromolecules, 1984 17(3): p. 332–336.

63. Audouin L, et al., Thickness distribution of degradation products during photochemical aging of rigid PVC. Die Angewandte Makromolekulare Chemie, 1998 261(1): p. 25–34.

64. Gardette J, Gaumet S, and Philippart J, Influence of the experimental conditions on the photooxidation of poly (vinyl chloride). Journal of applied polymer science, 1993 48(11): p. 1885–1895.

65. Schlagenhauf L, et al., Carbon nanotubes released from an epoxy-based nanocomposite: quantification and particle toxicity. Environmental science & technology, 2015 49(17): p. 10616–10623. [PubMed: 26251010]

66. Pathakoti K, et al., Photoinactivation of Escherichia coli by sulfur-doped and nitrogen-fluorine-codoped TiO2 nanoparticles under solar simulated light and visible light irradiation. Environ Sci Technol, 2013 47(17): p. 9988–96. [PubMed: 23906338]

67. Schlagenhauf L, et al., Carbon Nanotubes Released from an Epoxy-Based Nanocomposite: Quantification and Particle Toxicity. Environ Sci Technol, 2015 49(17): p. 10616–23. [PubMed: 26251010]

68. Pathakoti K, et al., Photoinactivation of Escherichia coli by sulfur-doped and nitrogen–fluorine-codoped TiO2 nanoparticles under solar simulated light and visible light irradiation. Environmental science & technology, 2013 47(17): p. 9988–9996. [PubMed: 23906338]

69. Jing H, Sahle-Demessie E, and Sorial GA, Inhibition of biofilm growth on polymer-MWCNTs composites and metal surfaces. Sci Total Environ, 2018 633: p. 167–178. [PubMed: 29573683]

70. Zhang C, et al., Flexible polyimide nanocomposites with DC bias induced excellent dielectric tunability and unique non-percolative negative-k towards intrinsic metamaterials. ACS Appl Mater Interfaces, 2018.

(a)

(b)
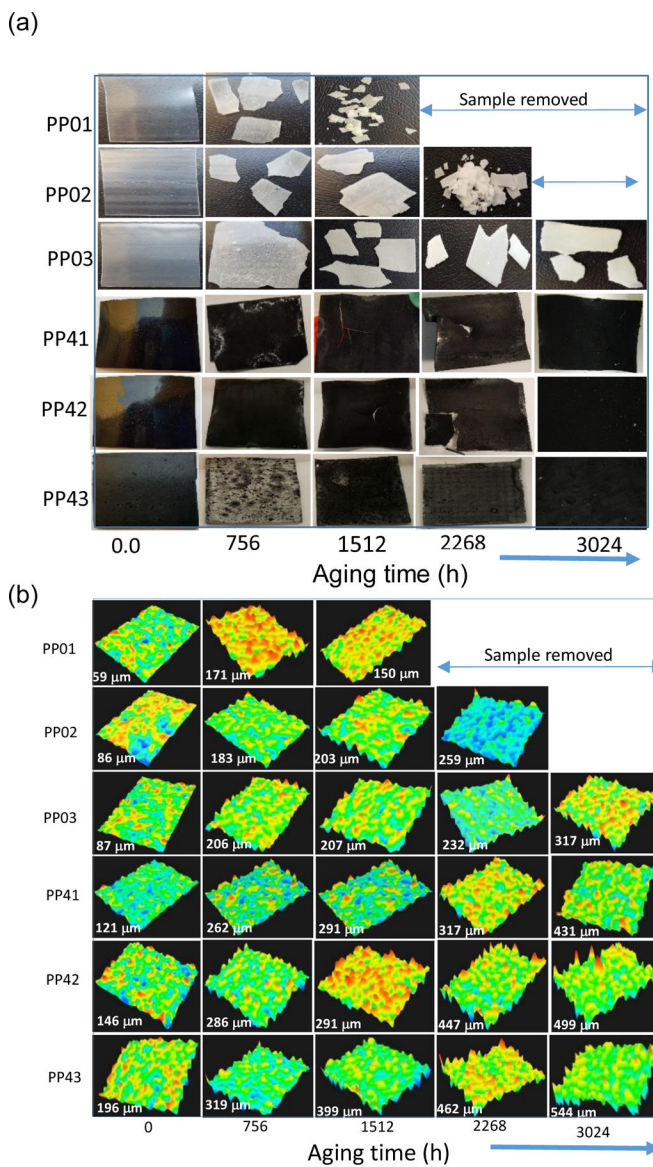
Figure 1.
(a) Optical photomicrographs of unfilled and MWCNT filled PP at selected exposure times
(b) 3D images and surface roughness of aged PP and PP-MWCNT composites during
weathering processes. Numbers show average surface roughness. PP01 and PP02 crumbled
after 1512 h ad 2268 h of the aging process.
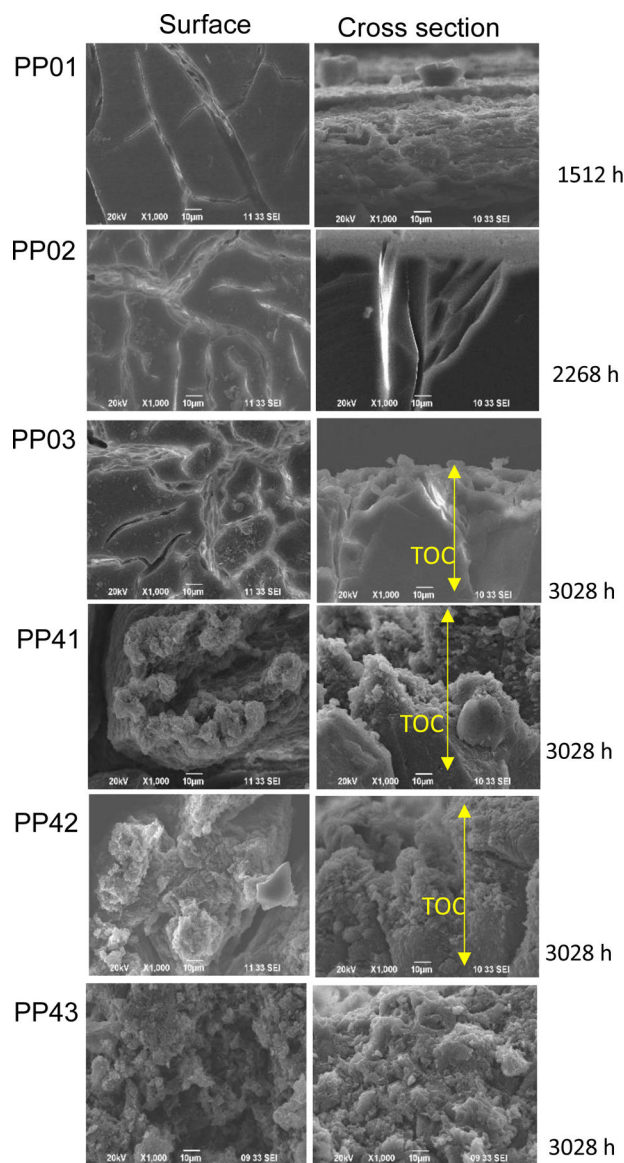
Figure 2.
Surface scanning electron micrographs of surface and cross-sectional images of polypropylene (PP01, PPO2, PP03) and PP-MWCNT (PP41, PP42, PP43) showing surface cracks the depth of the cracks.
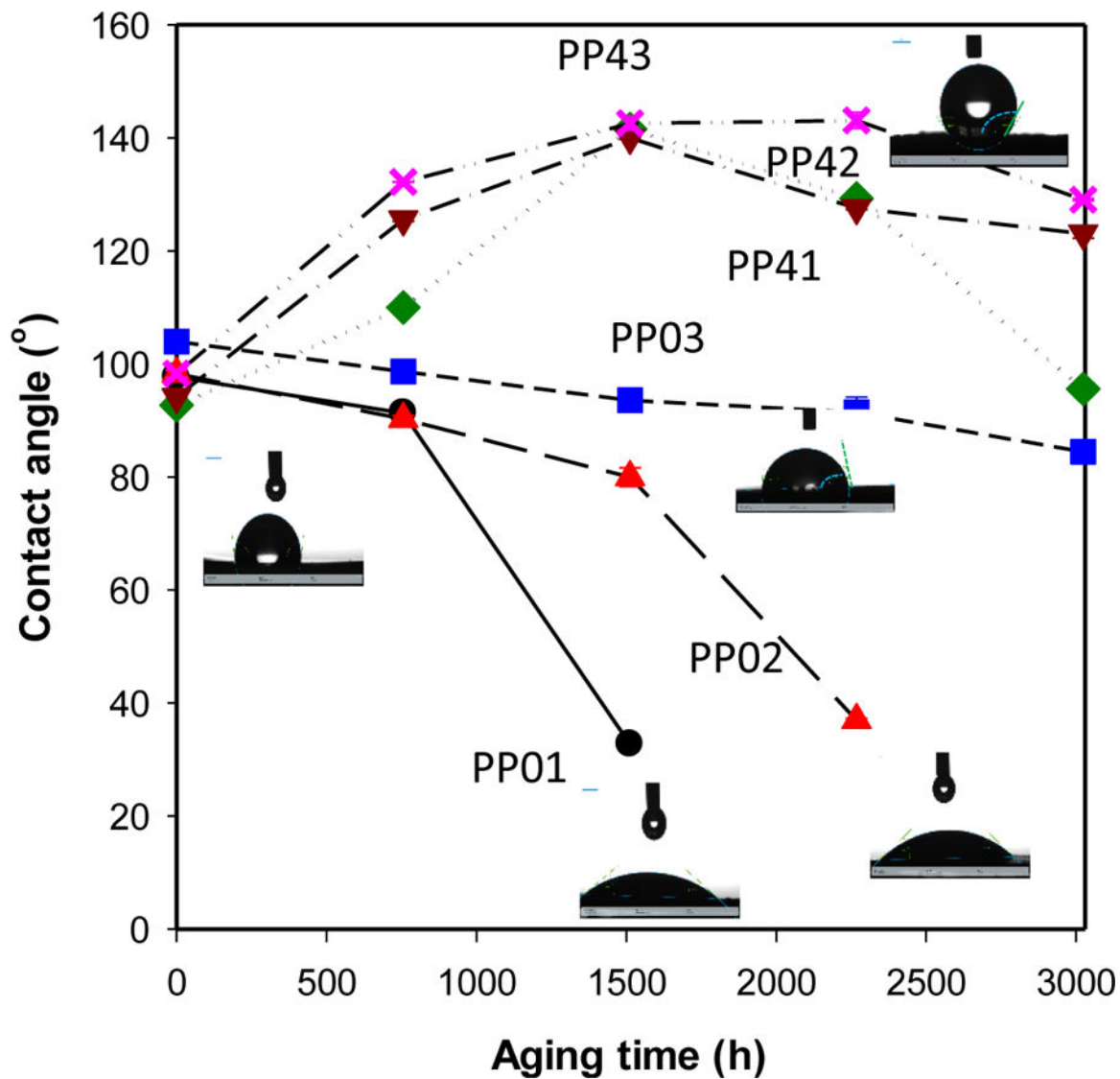
Figure 3.
Changes in contact angle during accelerated aging of PP and PP-MWCNT surfaces after selected degradation times, showing surface oxidation and erosion.
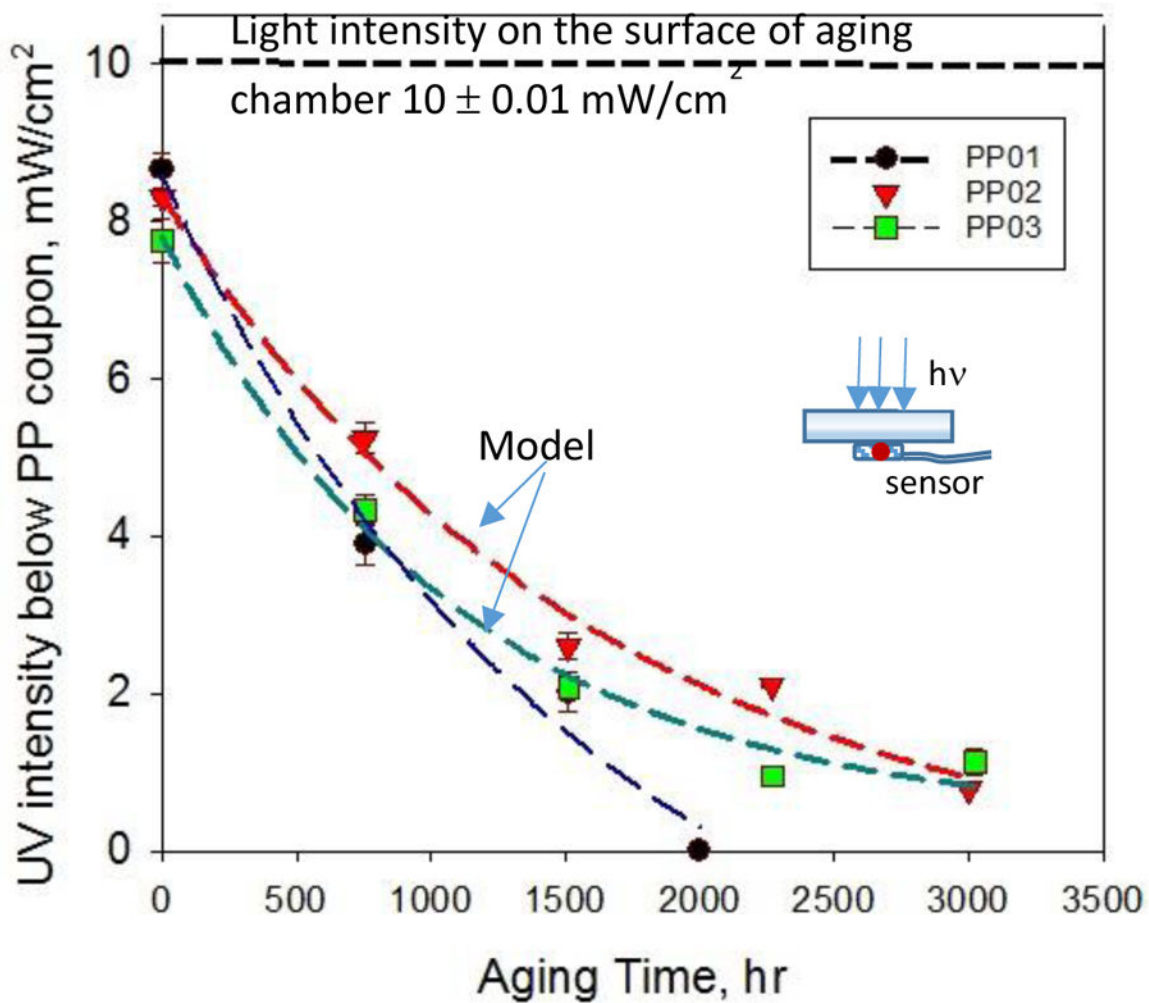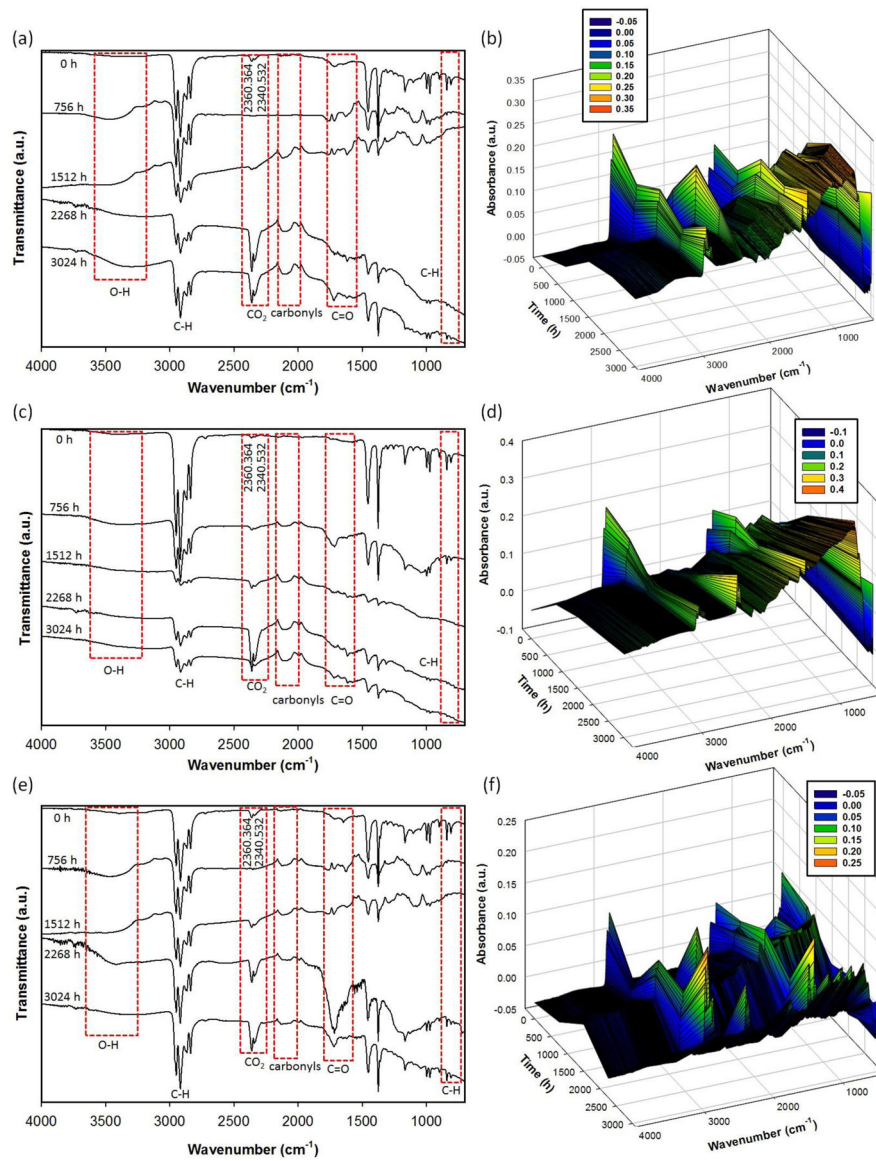
Figure 4.
Transmitted UV light through solar aged polypropylene coupons of different thicknesses.
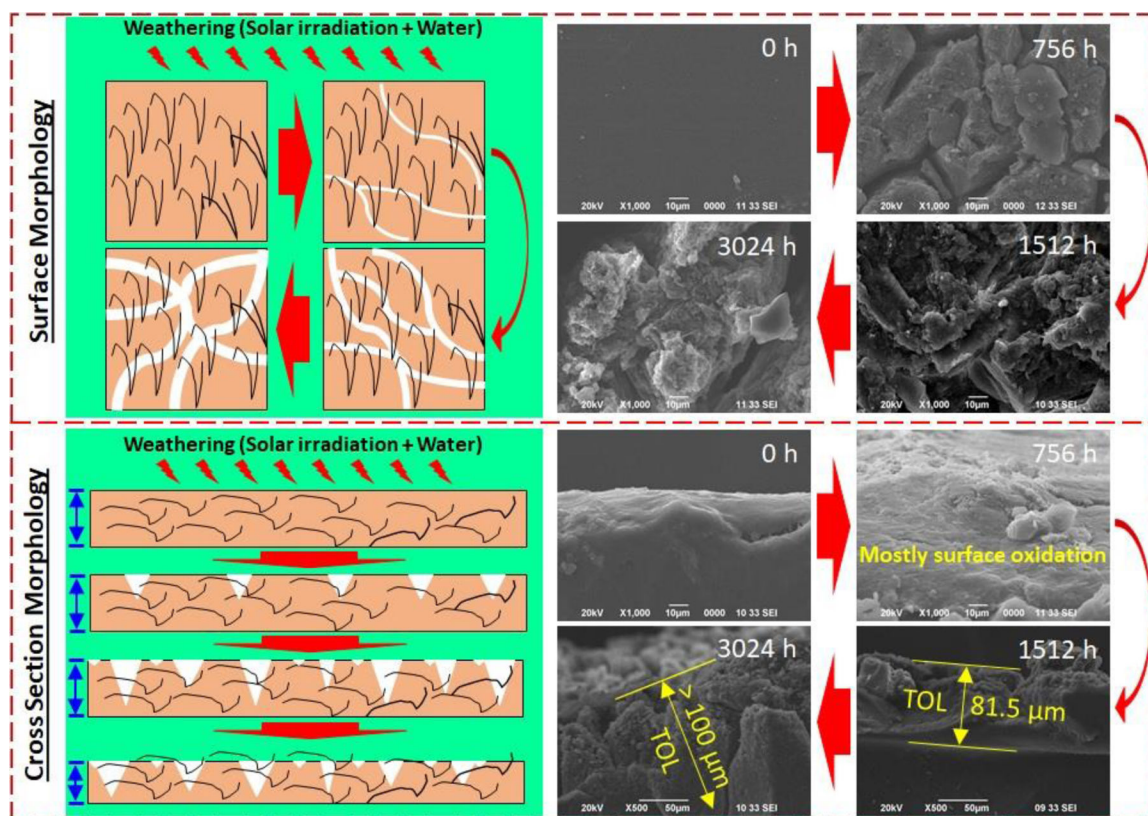Curves represent idealized chemical reaction unimpeded by diffusion.
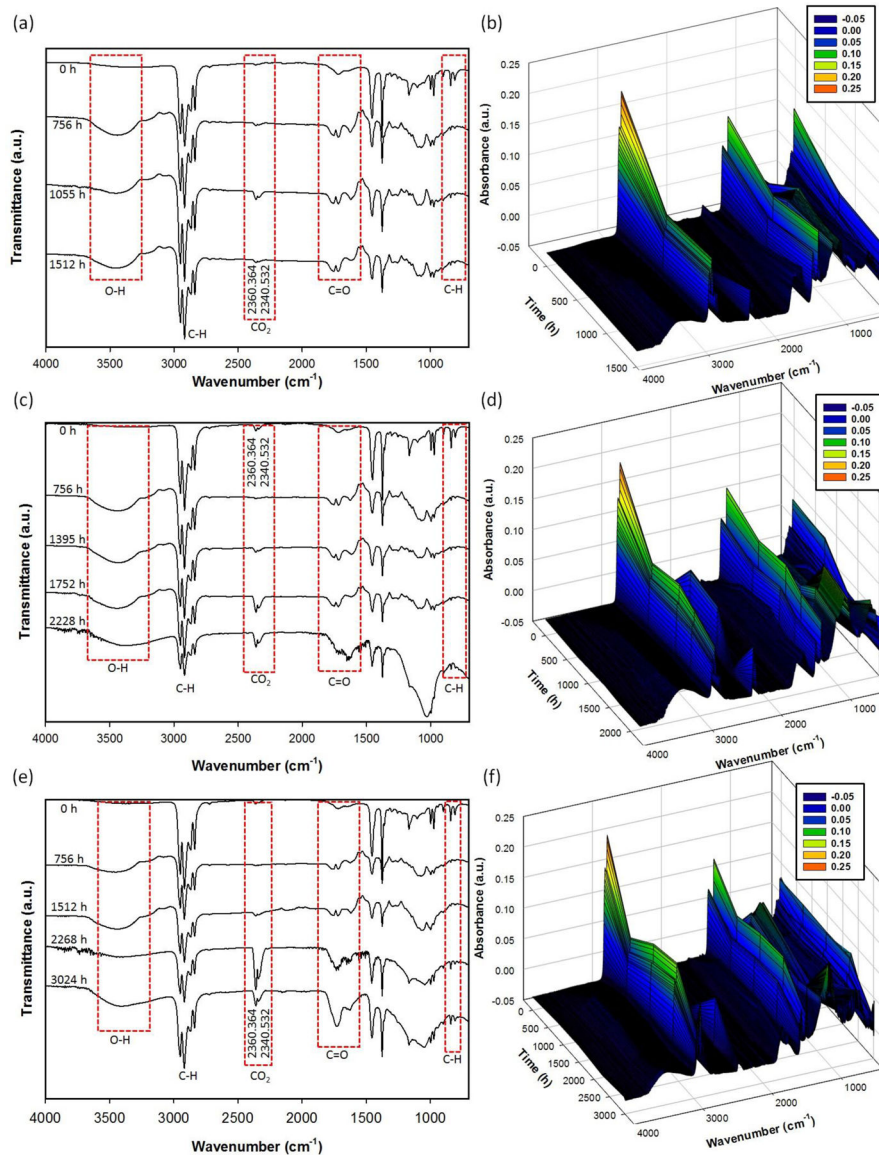
Figure 5.
2D and 3D FT-IR analysis for aged PP samples: (a) and (b) for aged PP01, (c) and (d) for aged PP02, and (e) and (f) for aged PP03.
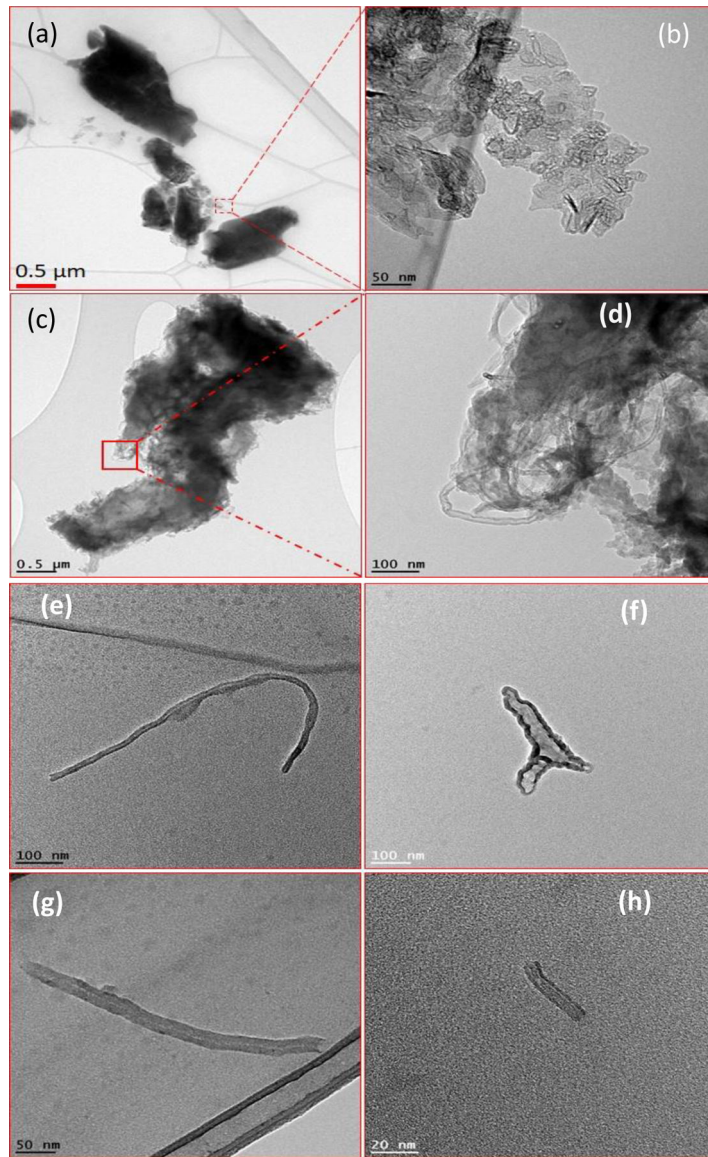
Figure 6.
Transmission FTIR and 3D FT-IR analysis for aged polypropylene-MWNT samples: (a) and
(b) for aged PP41, (c) and (d) for aged PP42, and (e) and (f) for aged PP43.
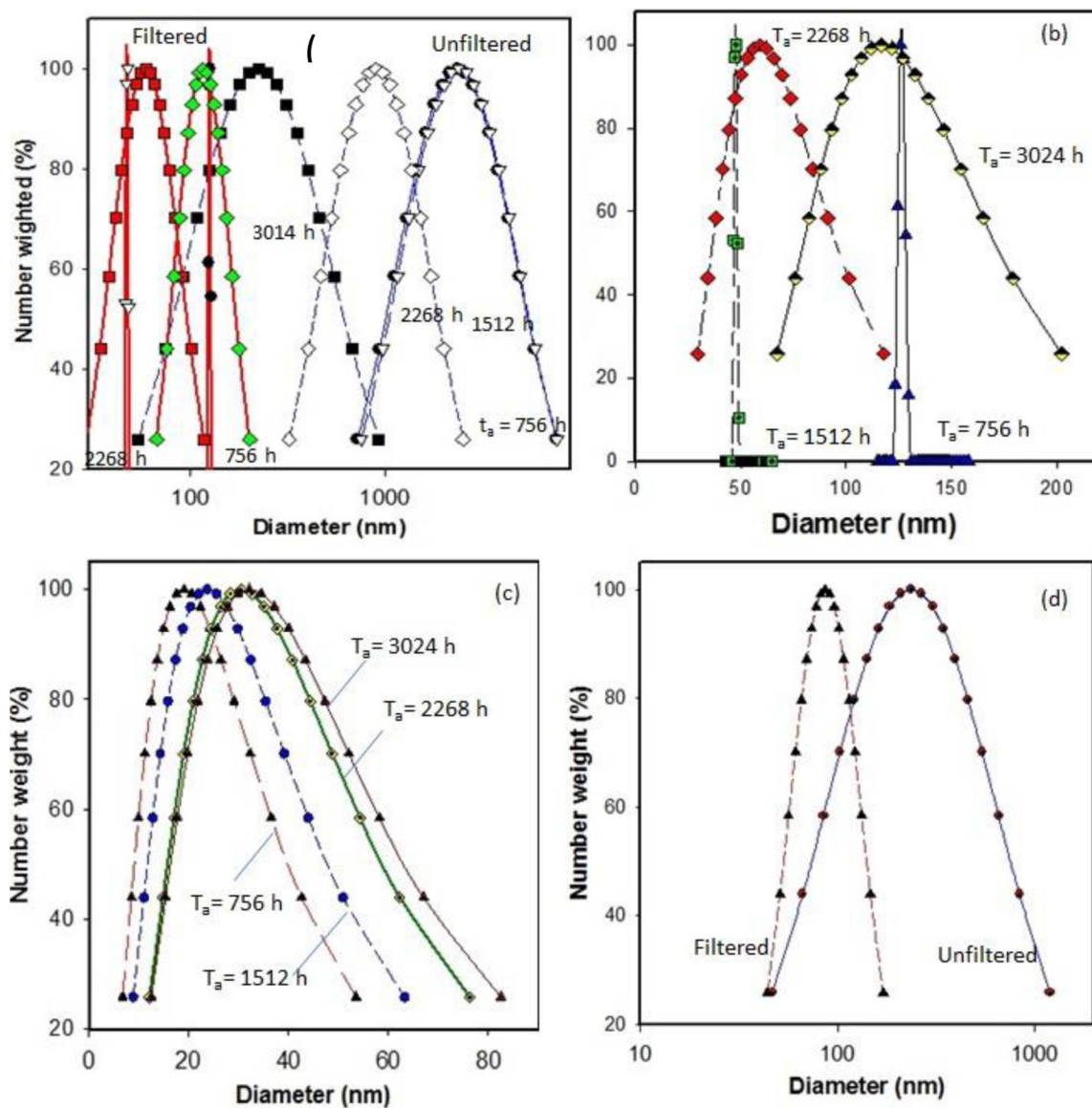
Figure 7.
A schematic (left) of degradation of PP-MWCNT nanocomposites by weathering and SEM images (right) of surface and cross-section of pristine and aged PP42. (TOL: Total oxidized layer).
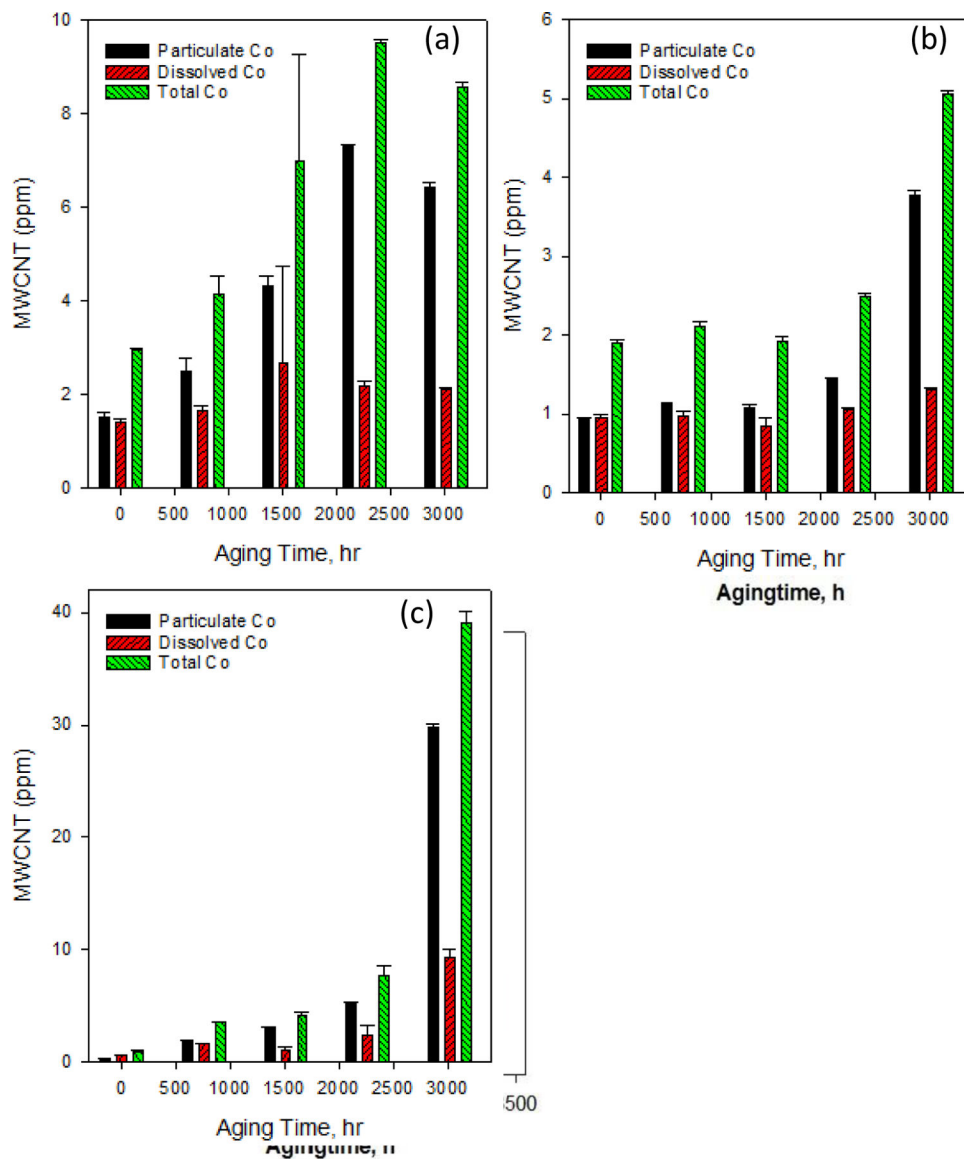
Figure 8.
Transmission electron micrograph images of released plastic fragments after (a) 1512 h and (b) 3012 h, containing MWCNTs from aged PP-MWCNTs composites, and images of released free MWCNTs from aged PP-MWCNT composites during washing after (e) and (f) 2268 h and (g) and (h) 3024 h.
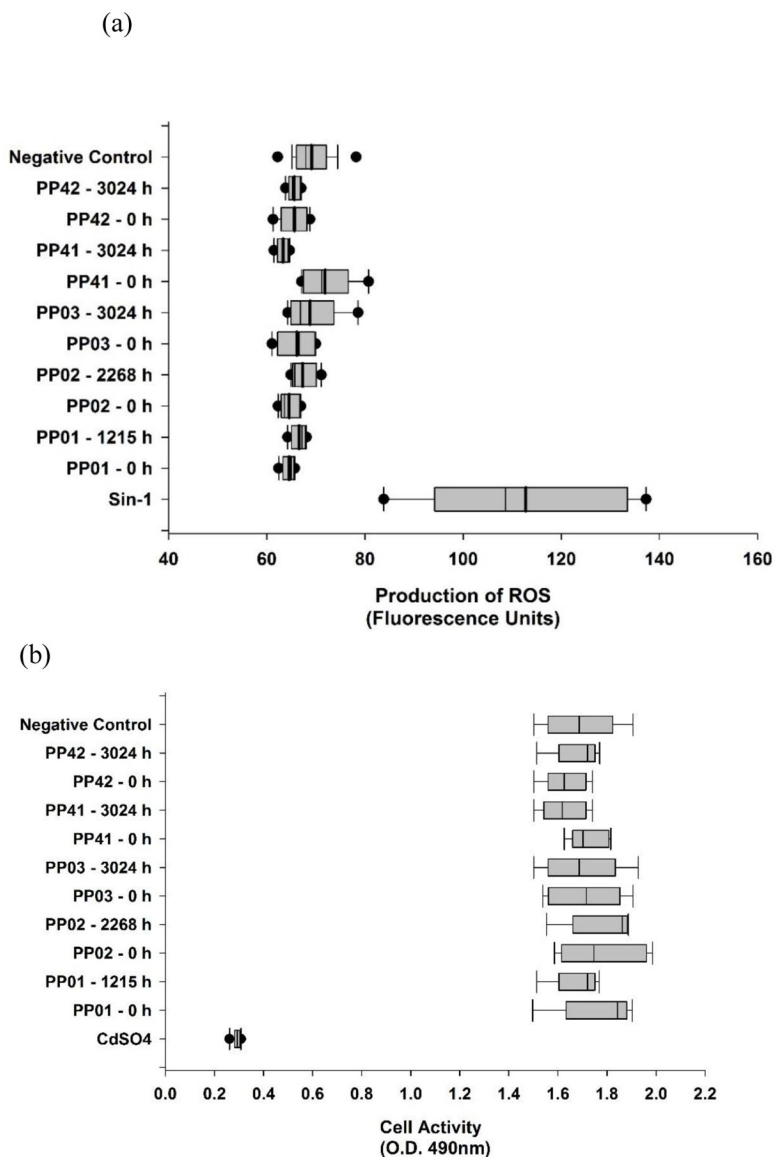
Figure 9.
Size distribution of released polymer fragments and nanoparticles determined using dynamic light scattering (a) before and after microfiltration using 0.45 μm filter, (b) released particles from PP41 after filtration, (c) released particles from PP42 after filtration, and (d) released particles from PP43 after filtration

Figure 10.
Estimated MWCNT determined using sp-ICP-MS that are released from aged
polypropylene-CNT composites (a) PP41 with thickness 0.25 ± 0.01, (b) PP42 with
thickness 0.50 ± 0.01, (c) PP43 with thickness 2.07 ± 0.06, that are aged for different
selected times.

(a)

(b)

Figure 11.
Intracellular formation of reactive oxygen species (ROS) and cell activity monitoring of A549 cells exposed to non-aged (0 h) and aged samples (maximum aged sample) of polypropylene and PP-MWCNT. Each assay had a positive control and negative control (a) Levels of ROS produced as measured by fluorescence units in the various samples. Sin-1 served as a positive control. (b) Cell viability and activity as determined by the production of formazan, after 24 h exposure to the various samples. $CdSO_4$ served as a positive control.

Table 1.

Prepared films of Polypropylene (PP) and PP-MWCNT nanocomposite

Material	Sample code	Thickness (mm)	MWCNT (%)
PP	PP01	0.25 ± 0.01	0
PP	PP02	0.39 ± 0.02	0
PP	PP03	0.69 ± 0.04	0
PP-MWCNT	PP41	0.35 ± 0.03	4
PP-MWCNT	PP42	0.50 ± 0.01	4
PP-MWCNT	PP43	2.07 ± 0.06	4

Table 2.

Experimental conditions for solar aging of PP and PP-MWCNT composite samples

Parameter	Condition
A cycle of weathering	120 min (Irradiation: 108 min and sprinkle: 12 min)
Humidity	8–20% for Sunshine and over 60% for Rain
Solar light irradiation	700 W/m^2
Wavelength of solar light	300–800 nm
Chamber Temperature	33–37 °C
Black Substance Temperature	65 °C

Table 3.

Sample aging time and converted real solar exposure time for the aging study

Aging time	Total solar radiant (MJ/m^2)	Real exposure time (Month)
756 h	1909.5	3.5
1512 h	3811.4	6.9
2268 h	5726.6	10.4
3024 h	7620.4	13.9